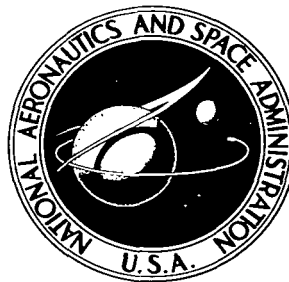


NASA TECHNICAL NOTE



NASA TN D-2570

e.1

NASA TN D-2570



A NUMERICAL METHOD FOR  
CALCULATING THE FLAT-PLATE  
PRESSURE DISTRIBUTIONS  
ON SUPERSONIC WINGS  
OF ARBITRARY PLANFORM

*by Wilbur D. Middleton and Harry W. Carlson*

*Langley Research Center*

*Langley Station, Hampton, Va.*

TECH LIBRARY KAFB, NM



0079667

A NUMERICAL METHOD FOR CALCULATING THE  
FLAT-PLATE PRESSURE DISTRIBUTIONS ON SUPERSONIC WINGS  
OF ARBITRARY PLANFORM

By Wilbur D. Middleton and Harry W. Carlson

Langley Research Center  
Langley Station, Hampton, Va.

NATIONAL AERONAUTICS AND SPACE ADMINISTRATION

For sale by the Office of Technical Services, Department of Commerce,  
Washington, D.C. 20230 -- Price \$1.00

A NUMERICAL METHOD FOR CALCULATING THE  
FLAT-PLATE PRESSURE DISTRIBUTIONS ON SUPERSONIC WINGS  
OF ARBITRARY PLANFORM

By Wilbur D. Middleton and Harry W. Carlson

SUMMARY

This report describes a numerical method based on linearized theory for calculating the flat-plate lifting-pressure distributions on supersonic wings of arbitrary planform, and presents examples illustrating its usage. The precision of the method is shown by comparisons of pressure distributions and force coefficients calculated from the numerical method with those obtained from established analytical solutions for straight-line leading- and trailing-edge wings. Several examples of the use of the numerical method to estimate the aerodynamic characteristics of curved or cranked leading-edge wings are presented to illustrate the flexibility of the method.

INTRODUCTION

A numerical method based on linear theory which allows the determination of camber surfaces corresponding to specified load distributions on supersonic wings of arbitrary planform (restricted only to supersonic trailing edges) has been presented in reference 1. The method substitutes approximate summations for linear-theory integral equations and replaces the wing with a mosaic of rectilinear elements closely approximating the wing planform. These substitutions allow great flexibility in defining both the planform shape and interval of integration for arbitrary wing planforms. The speed of present-day digital computers makes the solution practical.

An extension of the numerical method of reference 1 allows the calculation of the theoretical lifting-pressure distributions on flat wings of arbitrary planform (restricted to supersonic trailing edges). This report describes such a method and presents examples illustrating its use. The precision of the method is shown by comparisons of pressure distributions and force coefficients calculated from the numerical method with those determined from established analytical solutions for straight-line leading- and trailing-edge wings.

The further extension of the numerical method to the case of cambered wings is indicated.

## SYMBOLS

$A; A(L,N); A(L^*,N^*)$	leading-edge grid-element weighting factor
$\mathcal{AR}$	aspect ratio, $b^2/S$
$b$	wing span
$B; B(L^*,N^*)$	trailing-edge grid-element length
$\bar{c}$	mean aerodynamic chord
$C; C(L^*,N^*)$	grid-element width
$C_D$	drag coefficient
$C_L$	lift coefficient
$C_{L\alpha}$	slope of lift curve per degree angle of attack
$C_m$	pitching-moment coefficient about $x = 0$
$C_p$	pressure coefficient
$\Delta C_p$	lifting-pressure coefficient, $C_{p,lower} - C_{p,upper}$
$\overline{\Delta C_p}$	average value of lifting-pressure coefficient over a grid element (see eq. (7))
$\Delta C_{p,a}$	smoothed value of lifting-pressure coefficient obtained from averaged coefficients (see eq. (8))
$e/l$	notch ratio
$K$	a constant (see figs. 16 and 17)
$l$	overall length of wing, measured in streamwise direction
$L,N$	designation of influencing grid elements (see fig. 2)
$L^*,N^*$	designation of field-point grid elements (see fig. 2)
$M$	free-stream Mach number
$N_{max}$	value of $N$ at right-hand wing tip
$N_{min}$	value of $N$ at left-hand wing tip

R	influence function (see eq. (2))
$\bar{R}$	average value of influence function over a grid element (see eq. (5))
S	wing area
x, y, z	Cartesian coordinate system, X-axis streamwise
$x_{cp}$	distance from wing apex to center of pressure
$y_a$	apex spanwise position of M wing (see fig. 14)
$z_c$	camber surface ordinate
$\alpha$	wing angle of attack, deg
$\beta = \sqrt{M^2 - 1}$	
$\lambda$	wing taper ratio, $\frac{\text{Tip chord}}{\text{Root chord}}$
$\Lambda$	wing leading-edge sweepback angle
$\xi, \eta$	dummy variables of integration for x and y, respectively
$\tau$	denotes a region of integration bounded by wing planform and Mach forecone from point (x,y)
Subscripts:	
$L^*, N^*$	indicates value associated with element row (see eq. (14))
le	value of a quantity along wing leading edge at $\beta y = N$
te	value of a quantity along wing trailing edge at $\beta y = N$
$\infty$	corresponds to case of two-dimensional wing

#### NUMERICAL CALCULATION METHOD

The numerical method for calculating the theoretical lifting pressure distributions on supersonic wings employs a basic equation of linear theory (eq. (77a) of ref. 2) which relates the local surface slope of a point on a lifting surface to the pressure coefficient at the point, the influence of

pressures upstream of the specified point being taken into account. The method employed herein actually is an extension of the numerical method of reference 1, in which the wing surface shape necessary to support a specified lift distribution is calculated.

A typical wing planform of arbitrary shape, defined by a rectangular Cartesian coordinate system, is shown in figure 1. In accordance with the concepts of linearized theory, the wing is assumed to have negligible thickness and is assumed to lie approximately in the  $z = 0$  plane. The wing surface is flat and at a slight incidence to the local flow. The trailing edge of the wing is supersonic.

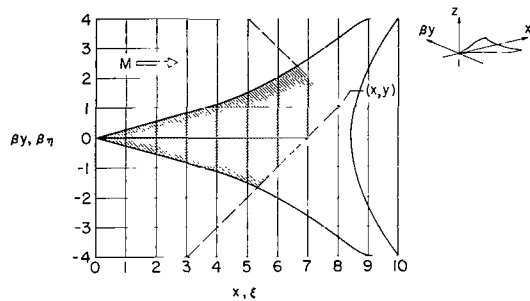


Figure 1. - Cartesian coordinate system.

Equation (2) of reference 1 may be rearranged to solve for the lifting-pressure coefficient at the field point  $(x,y)$  as

$$\Delta C_p(x,y) = - \frac{4}{\beta} \frac{\partial z_c}{\partial x}(x,y) + \frac{1}{\pi} \int d\xi \int_{\tau} R(x-\xi, y-\eta) \Delta C_p(\xi, \eta) d\beta\eta \quad (1)$$

where values of  $\Delta C_p(\xi, \eta)$  in the integrand are previously determined values of  $\Delta C_p(x,y)$  as discussed subsequently. The region of integration  $\tau$  extends over the wing planform within the Mach forecone from point  $(x,y)$ , as shown by the shaded region of figure 1. The wing streamwise slope function  $\frac{\partial z_c}{\partial x}(x,y)$  is a constant for the flat plate at incidence  $\left(\frac{dz_c}{dx}\right)$  and is equal to the tangent of the wing angle of attack.

The special integral sign  $\int$  of equation (1) denotes that only the generalized principal part (see refs. 2 and 3) of the integral is of interest, which permits an evaluation of the integral across the singularity at  $y = \eta$ . The numerical method substitutes a summation for the integral of equation (1), consisting of the sum of an average pressure coefficient times the integral of the  $R$  function over the grid elements within  $\tau$ . The  $R$  function, which may be thought of as an influence factor relating the upstream pressures to the lifting pressure at point  $(x,y)$ , is defined as

$$R(x-\xi, y-\eta) = \frac{x - \xi}{\beta^2(y - \eta)^2 \sqrt{(x - \xi)^2 - \beta^2(y - \eta)^2}} \quad (2)$$

In integrating the R function over the individual elements, the integral is regular except for the elements containing  $y = \eta$ , which require the definition of the generalized principal part. The integral of the R function for these elements is more readily evaluated if the  $\eta$  limits are chosen as  $\eta - \delta$  and  $\eta + \delta$ . With the grid system oriented to provide this choice of limits, the integral of the R function over the elements containing  $y = \eta$  becomes the definite integral of the function with the infinite portion discarded. (See ref. 2 or 3.)

As in reference 1, the grid system of the numerical method is superimposed upon the wing planform as shown in figure 2, with grid elements identified by L and N replacing the integral elements  $d\xi$  and  $d\beta\eta$ . Along the wing leading and trailing edges, partial grid elements are used to improve the planform definition. Values of  $L^*$  and  $N^*$  identify the grid element associated with and immediately forward of the field point  $(x,y)$ . The grid element  $L^*$  is numerically equal to  $x$  and the grid element  $N^*$  is numerically equal to  $\beta y$ , where  $x$  and  $\beta y$  take on only integer values. The area of integration of the numerical method consists of a group of grid elements approximating  $\tau$  as shown by the shaded region of figure 2. The grid element system illustrated in figure 2 is rather coarse; in practice, many more elements are employed.

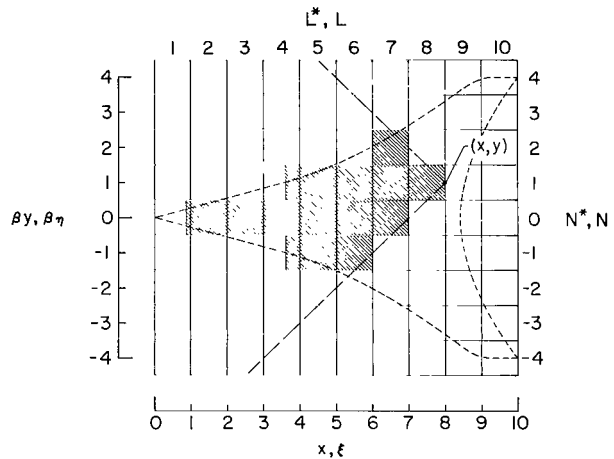


Figure 2.- Grid system used in numerical solution.

The numerical summation treats the integration interval element by element, with the average lifting-pressure coefficient  $\overline{\Delta C_p}(L,N)$  over the element being multiplied by  $\overline{R}$ , the average value of the influence function over the same grid element. The contribution of an individual element  $(L,N)$  to the lifting-pressure coefficient at point  $(x,y)$  may be expressed by

$$\frac{1}{\pi} \overline{R}(L^*-L, N^*-N) A(L,N) \overline{\Delta C_p}(L,N) \quad (3)$$

The weighting factor  $A(L,N)$  accounts for fractional elements along the wing leading edges as follows:

$$\left. \begin{aligned} A(L,N) &= 0 && (L < L_{1e}) \\ A(L,N) &= L - x_{1e} && (L = L_{1e}) \\ A(L,N) &= 1 && (L > L_{1e}) \end{aligned} \right\} \quad (4)$$

where  $L_{1e}$  is numerically equal to the whole number part of the sum  $x_{1e} + 1$ , or  $1 + [x_{1e}]$ . The bracket notation is used to signify that only the whole number part of the number is retained.

Since it has been observed that an integration of equation (2) is relatively insensitive to small variations in  $\xi$ , the integral of the function  $R$  over an individual element may be approximately evaluated with the value  $x - \xi$  equal to its average value  $L^* - L + 0.5$ . (See ref. 1.) The resulting expression for the average influence factor  $\bar{R}$  is:

$$\bar{R}(L^*-L, N^*-N) = \frac{\sqrt{(L^* - L + 0.5)^2 - (N^* - N - 0.5)^2}}{(L^* - L + 0.5)(N^* - N - 0.5)} - \frac{\sqrt{(L^* - L + 0.5)^2 - (N^* - N + 0.5)^2}}{(L^* - L + 0.5)(N^* - N + 0.5)} \quad (5)$$

A graphical representation of this factor is shown in figure 3. The values of  $\bar{R}$  between the limits of the Mach forecone at a constant  $(L^* - L)$  station sum to zero, the positive values canceling the single negative value at  $N^* = N$ . At  $L^* = L$ , where the forecone includes only one element,  $\bar{R}$  is zero.

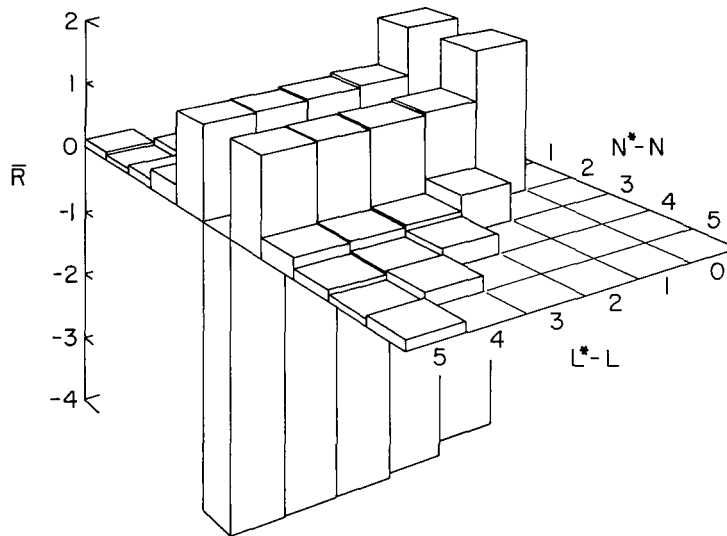


Figure 3.- Distribution of  $\bar{R}$  function.

With the integral of equation (1) replaced by the combined contribution of all elements within  $\tau$ , the lifting-pressure coefficient at element  $(L^*, N^*)$  is

$$\Delta C_p(L^*, N^*) = -\frac{4}{\beta} \frac{dz_c}{dx} + \frac{1}{\pi} \sum_{N_{\min}}^{N_{\max}} \sum_{L_{1e}}^{L^* - |N^* - N|} \bar{R}(L^* - L, N^* - N) A(L, N) \Delta C_p(L, N) \quad (6)$$

The vertical lines used in  $|N^* - N|$  designate the absolute value of the enclosed quantity. The limits on  $L$  in the summation are those of the wing leading edge and the Mach forecone at a selected  $N$  value.

The calculation of  $\Delta C_p(L^*, N^*)$  requires the prior determination of all values of  $\overline{\Delta C_p}(L, N)$  within the region of integration (where  $\overline{\Delta C_p}$  is an average value of pressure coefficient over a grid element obtained from  $\Delta C_p$ , as discussed subsequently). The order of calculation of  $\Delta C_p(L^*, N^*)$  is from apex aft (i.e., increasing values of  $L^*$ ); thus, all pressure coefficients within the Mach forecone from any element have been previously obtained and no unknown pressure coefficients arise in the summation. Since the value of  $\overline{R}(L^*, N^*)$  is zero,  $\overline{\Delta C_p}(L^*, N^*)$  in the summation is not required.

Theoretically,  $\Delta C_p(L^*, N^*)$  defined by equation (6) is the pressure coefficient at the aft midpoint of the  $L^*, N^*$  element. This value, however, is not as representative of the average value of  $\Delta C_p$  over the element as is the value of  $\Delta C_p$  at the center of the element. An approximate average value,  $\overline{\Delta C_p}(L^*, N^*)$ , is obtained by linearly interpolating along  $N^*$  for the pressure coefficient at the midpoint of  $L^*, N^*$  and is based on the calculated value of  $\Delta C_p(L^*, N^*)$  and the previously averaged value of  $\overline{\Delta C_p}(L^*-1, N^*)$  of the grid element immediately forward of  $L^*, N^*$ :

$$\overline{\Delta C_p}(L^*, N^*) = \frac{2}{3} \Delta C_p(L^*, N^*) + \frac{1}{3} \overline{\Delta C_p}(L^*-1, N^*) \quad (L^* > L_{1e}) \quad (7a)$$

When  $L^*$  is the leading-edge block of  $N^*$ , the value of  $\overline{\Delta C_p}(L^*, N^*)$  is considered equal to the calculated value of  $\Delta C_p(L^*, N^*)$ ; that is,

$$\overline{\Delta C_p}(L^*, N^*) = \Delta C_p(L^*, N^*) \quad (L^* = L_{1e}) \quad (7b)$$

In the development of the numerical method described in this report, it was found that  $\overline{\Delta C_p}$ , when integrated over the wing planform, produced lift coefficients and center-of-pressure locations in good agreement with those obtained from established analytical solutions. However, comparisons between the detailed pressure distributions determined by the numerical method and those obtained from the analytical solution were poor (for most wing planforms); especially for sweptback subsonic leading-edge wings, where theoretically an infinite pressure coefficient is obtained at the leading edge, the numerical-method pressure distributions fluctuated considerably about an approximate mean defined by the analytical solution.

In order to reduce local oscillations in pressure from element to element and to permit critical comparisons between pressure distributions obtained from the numerical method and those obtained from the analytical solutions, a "smoothing" operation was performed upon the  $\overline{\Delta C_p}$  values. For use in this operation a number of experimental-data smoothing techniques were tried, in which a weighted mean of a group of values is calculated. The equation selected was a nine-point smoothing formula operating along a constant  $N^*$  value:

$$\Delta C_{p,a}(L^*, N^*) = \frac{\left\{ \begin{array}{l} 0.2A(L^*-4, N^*) \overline{\Delta C_p}(L^*-4, N^*) + 0.4A(L^*-3, N^*) \overline{\Delta C_p}(L^*-3, N^*) + 0.6A(L^*-2, N^*) \overline{\Delta C_p}(L^*-2, N^*) \\ + 0.8A(L^*-1, N^*) \overline{\Delta C_p}(L^*-1, N^*) + A(L^*, N^*) \overline{\Delta C_p}(L^*, N^*) + 0.8\overline{\Delta C_p}(L^*+1, N^*) \\ + 0.6\overline{\Delta C_p}(L^*+2, N^*) + 0.4\overline{\Delta C_p}(L^*+3, N^*) + 0.2\overline{\Delta C_p}(L^*+4, N^*) \end{array} \right\}}{0.2A(L^*-4, N^*) + 0.4A(L^*-3, N^*) + 0.6A(L^*-2, N^*) + 0.8A(L^*-1, N^*) + A(L^*, N^*) + 2.0} \quad (8)$$

where the A value is the grid-element factor as defined in equation (4) (with  $A = 1$  for  $L^* > L_{1e}$ ).

The nine-point smoothing formula was found superior to techniques which employed both spanwise and chordwise smoothing, to techniques which utilized additional averaging terms in the calculation of  $\overline{\Delta C_p}(L^*, N^*)$ , and to techniques which used different sets of grid elements along  $N^*$ . The important feature of the smoothing technique was the inclusion of a sufficient number of chordwise grid elements to approach satisfactorily a local mean value. The smoothing equation is not used in the calculation of the wing pressure coefficients (eq. (6)), but is employed after  $\overline{\Delta C_p}(L^*, N^*)$  has been computed for the entire wing planform. However, since the nine-point formula requires four grid elements aft of element  $(L^*, N^*)$ , the wing planform is extended four elements aft of the actual wing trailing edge. This step is permissible since the wing trailing edge is required to be supersonic.

Since the smoothing is applied only along constant  $N^*$  stations, erratic behavior of the pressure coefficients might be expected in cross plots at constant  $L^*$  stations. Such is not the case, as shown subsequently, except in the limiting condition of a sonic leading edge, which offers no difficulty if the leading edge is only slightly supersonic or slightly subsonic.

The general effect of the nine-point smoothing technique, aside from the improvement in detailed pressure distributions, is a slight resultant decrease in the integrated wing force coefficients. The percentage decrease is a function of the size of the wing (number of grid elements used) and the degree of leading-edge sweepback. For typical wings of interest, the decrease averages approximately 2 to 4 percent for the lift, drag, and pitching-moment coefficients, with little effect on the center of pressure.

Calculations of the wing force coefficients require appropriate area and lifting-pressure summations, which are limited to the right-hand wing panel because of symmetry. Since only the smoothed pressure distributions are of interest, force coefficients based on  $\Delta C_{p,a}$  are calculated.

The wing area may be found through a summation as follows:

$$S = \frac{2}{\beta} \sum_{N^*=0}^{N^*=N_{\max}} \sum_{L^*=L_{1e}}^{L^*=L_{te}} A(L^*,N^*) B(L^*,N^*) C(L^*,N^*) \quad (9)$$

where

$L_{1e}$  leading-edge grid element,  $1 + [x_{1e}]$

$L_{te}$  trailing-edge grid element,  $1 + [x_{te}]$

A,B,C leading-edge, trailing-edge, and center-line or wing-tip grid-element fractions, respectively

The leading-edge grid-element fraction is defined by equation (4), the trailing-edge grid-element length is defined by

$$\left. \begin{aligned} B &= 1 & (L^* < L_{te}) \\ B &= x_{te} + 1 - L_{te} & (L^* = L_{te}) \end{aligned} \right\} \quad (10a)$$

and the center-line or wing-tip grid-element width is defined by

$$\left. \begin{aligned} C &= 0.5 & (N^* = 0) \\ C &= 1 & (0 < N^* < N_{\max}) \\ C &= 0.5 & (N^* = N_{\max}) \end{aligned} \right\} \quad (10b)$$

The lift coefficient may be obtained from the following summation:

$$C_L = \frac{2}{\beta S} \sum_{N^*=0}^{N^*=N_{\max}} \sum_{L^*=L_{1e}}^{L^*=L_{te}} \Delta C_{p,a}(L^*,N^*) A(L^*,N^*) B(L^*,N^*) C(L^*,N^*) \quad (11)$$

The pitching-moment coefficient about  $x = 0$  is

$$C_m = \frac{2}{\beta S \bar{c}} \sum_{N^*=0}^{N^*=N_{\max}} \sum_{L^*=L_{1e}}^{L^*=L_{te}} (L^* - 0.5) \Delta C_{p,a}(L^*, N^*) A(L^*, N^*) B(L^*, N^*) C(L^*, N^*) \quad (12)$$

The drag coefficient may be expressed as follows:

$$C_D = -C_L \frac{dz_c}{dx} \quad (13)$$

This relationship does not consider any contribution of the theoretical "leading-edge-suction" force and accounts only for the inclination of the normal force to the relative wind.

The distribution of wing lift in the streamwise and spanwise direction may be obtained from summations, taken row by row, of grid element forces in the L- and N-direction, respectively. These distributions are conveniently expressed as fractions of total wing lift as follows:

For the streamwise lift distribution,

$$\frac{\text{Lift}_{L^*}}{\text{Total lift}} = \frac{2 \sum_{N^*=0}^{N^*=N_{\max}} \Delta C_{p,a}(L^*, N^*) A(L^*, N^*) B(L^*, N^*) C(L^*, N^*)}{\beta C_L S} \quad (14a)$$

and for the spanwise lift distribution, at a selected  $N^*$  value on the right-hand wing panel only,

$$\frac{\text{Lift}_{N^*}}{\text{Total lift}} = \frac{\sum_{L^*=L_{1e}}^{L^*=L_{te}} \Delta C_{p,a}(L^*, N^*) A(L^*, N^*) B(L^*, N^*) C(L^*, N^*)}{\beta C_L S} \quad (14b)$$

#### EXTENSION OF NUMERICAL CALCULATION METHOD

The method for calculating the lifting-pressure coefficients on supersonic wings outlined in the preceding section has been restricted to the case of flat

wings by restricting the wing streamwise slope function  $\frac{\partial z_c}{\partial x}(x,y)$  to a constant (equal to the tangent of the wing angle of attack). The same calculation method could be extended to the case of wings having cambered surfaces by considering  $\frac{\partial z_c}{\partial x}$  to be a function of the  $x$  and  $y$  planform coordinates. This extension would require only the addition of a suitable method for providing the variable slope term to be used with the grid-element system, that is, supplying an appropriate function  $\frac{\partial z_c}{\partial x}(L^*, N^*)$ .

## COMPARISONS AND EXAMPLES

Several comparisons of lifting-pressure distributions and wing force coefficients calculated from the numerical method with those obtained from established analytical solutions are presented in this section to illustrate the precision of the numerical method. Also, several examples of the use of the numerical method to estimate the aerodynamic characteristics of curved or cranked leading-edge wings are presented to illustrate the flexibility of the method.

The data obtained from the numerical method were calculated on a digital computer, programed to employ the equations presented in the section entitled "Numerical Calculation Method." In the figures presenting the pressure-distribution comparisons, the numerical-method pressure coefficients are the smoothed values.

### Comparison of Numerical Method With Analytical Solutions

Several comparisons between the numerical-method solutions and established analytical solutions may be made for delta-wing planforms, with various orientations between the wing apex half-angle and the apex Mach line. Figure 4 shows the lift-curve slope and streamwise center-of-pressure location for a delta-wing planform as a function of the leading-edge sweepback parameter  $\beta \cot \Lambda$ .

The numerical-method data agree quite well with the theoretical solution of reference 4, with the exception of the sonic leading-edge wing ( $\beta \cot \Lambda = 1.0$ ). The sonic leading-edge wing is a limiting condition for the numerical method, as discussed subsequently, although only slightly subsonic or slightly supersonic leading-edge wings offer no difficulty. A tendency of the numerical method to give slightly lower lift-curve slopes than those obtained from the theory of reference 4 may be observed for the subsonic leading-edge condition. This effect is primarily attributed to a flattening of the leading-edge pressure peaks (theoretically infinite) caused by the averaging techniques.

The force data from the numerical method are affected, to some extent, by the number of grid elements chosen to represent the wing. The width of the wing semispan, in  $\beta y$  grid elements, for most of the delta-planform series was

$N_{max} = 50$ , which defined in turn the wing length. Wings with small values of  $\beta \cot \Lambda$ , that is, 0.20 or 0.40, are very long (in L units) if scaled to a 50-unit semispan; therefore, in calculating the data for these wings, semispan widths of 10 and 20 units, respectively, were used.

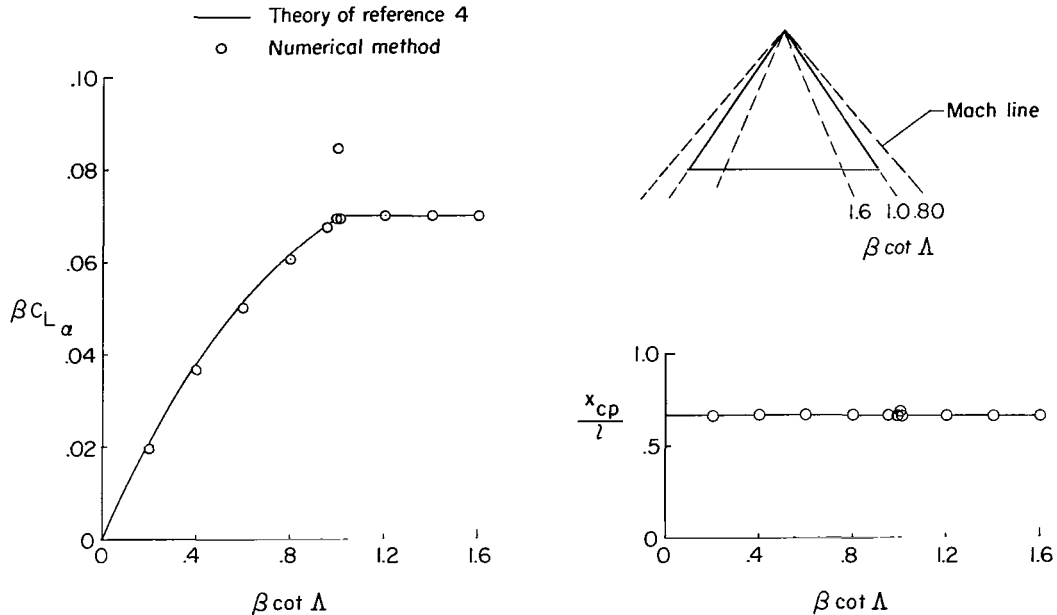


Figure 4.- Aerodynamic characteristics of delta wing.

The basic consideration in scaling the wing for the computer program is calculation time. A delta wing with approximately 1200 grid elements representing the semispan requires on the order of 15 minutes calculation time on a high-speed digital computer. Larger wing areas require proportionately longer calculation time, although both wing area and average chord length affect the time required.

The effect of  $N_{max}$  on the wing lift-curve slope is shown in figure 5 for a representative delta wing with  $\beta \cot \Lambda = 1.60$  and  $\beta \cot \Lambda = 0.80$ . Only very minor changes in the lift-curve slope occur when the number of grid elements is greater than  $N_{max} \approx 20$ . On the basis of the data of figure 5, the more complicated planform shapes of this report were scaled to a value of  $N_{max}$  on the order of 50 units for the computer program.

Comparisons of detailed lifting pressure distributions between the numerical method and the data of reference 4 for the delta wing at several values of  $\beta \cot \Lambda$  are presented in figures 6 to 8.

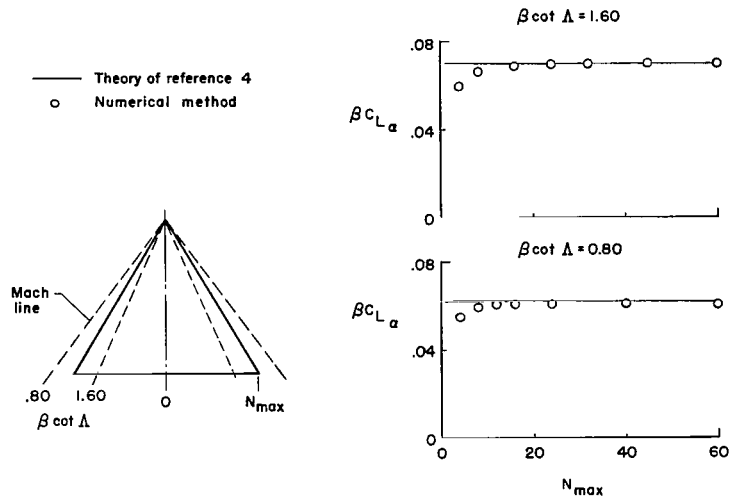


Figure 5.- Effect of  $N_{max}$  on lift-curve slope of representative delta wing.

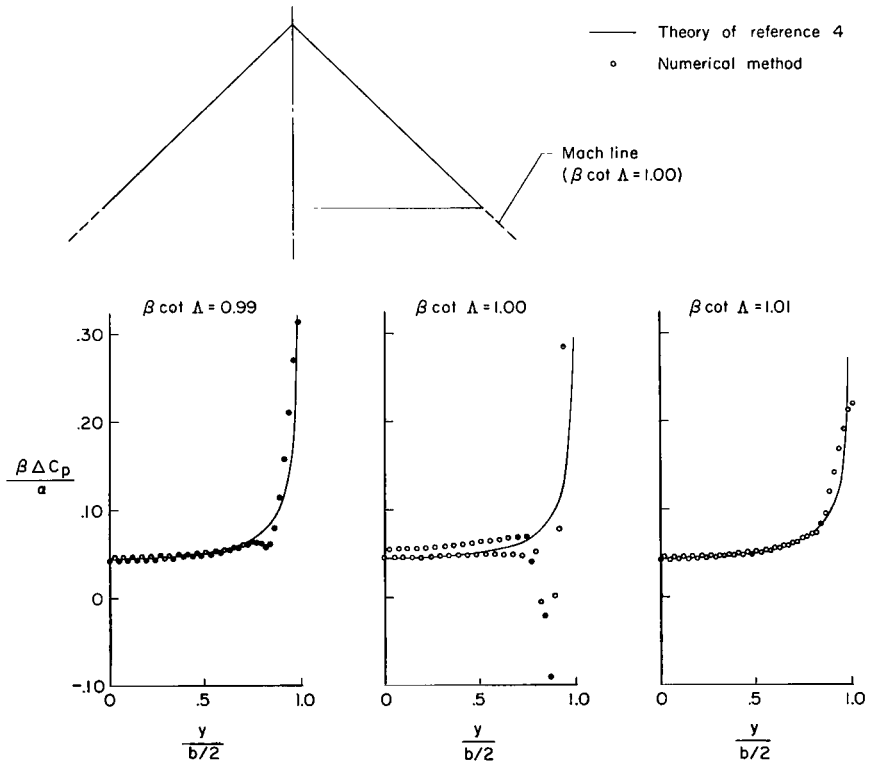


Figure 6.- Lifting-pressure distributions at and near sonic leading-edge condition for delta wing.  $x/l = 1.0$ ;  $N_{max} = 50$ .

Lifting-pressure data for a delta wing with a sonic leading-edge condition ( $\beta \cot \Lambda = 1.00$ ) and two near-sonic leading-edge conditions ( $\beta \cot \Lambda = 0.99$  and  $\beta \cot \Lambda = 1.01$ ) are presented in figure 6. In all three cases, spanwise oscillations of the lifting-pressure data (at  $x/l = 1.0$ ) occur and they become so large as to invalidate the total wing force coefficients for the sonic leading-edge case. These oscillations damp out rapidly for leading-edge flow conditions which are only slightly different from the sonic case, so that, for practical purposes, wing planforms with sonic leading-edge conditions can be studied through only slight alteration of the leading-edge sweepback parameter.

The case of a subsonic leading-edge wing ( $\beta \cot \Lambda = 0.80$ ) is illustrated in figure 7. A staggered ordinate scale is used in figure 7 (and in several subsequent figures) to separate the comparisons for spanwise cuts at several  $x/l$  stations. In general, good agreement is obtained between the numerical and analytical solutions, although some unevenness is apparent in the numerical data. The data of figure 7 could be considered to be those of the apex region of a much larger (longer and wider) wing having the same sweepback parameter but at correspondingly reduced values of  $x/l$ . Enlarging the wing size would improve the detailed-pressure-coefficient comparisons at a given  $x/l$ , but would require longer calculation time without appreciable effect on the integrated wing force coefficients.

Lifting-pressure distributions for a supersonic leading-edge delta wing ( $\beta \cot \Lambda = 1.20$ ) are shown in figure 8. Agreement between the numerical and analytical solutions in this case is quite good, although the numerical method does not exhibit the sharp break at the Mach line characteristic of the analytical solution. The unevenness of the pressure coefficients observed in the subsonic leading-edge case does not occur because of the reduced effect of the averaging techniques with the less severe leading-edge pressures.

Comparisons between the numerical method and the theory of reference 5 for rectangular wings is presented in figures 9 and 10.

Lifting-pressure distributions for a rectangular wing of  $\beta AR = 1.0$  are presented in figure 9 for cuts at representative lengthwise stations. In this figure, the pressure coefficients are divided by the two-dimensional values acting on the forward part of the wing within the leading-edge Mach lines. The numerical data agree reasonably well with corresponding data from reference 5 but exhibit some effect of the number of grid elements used.

Figure 10 illustrates the general effect of the number of spanwise elements  $N_{max}$  on rectangular-wing data obtained for a wing of  $\beta AR = 2.0$  having semi-span widths of 10, 20, and 40 grid elements. Since the  $\Delta C_{p,a}$  values of the numerical method occur at different  $x/l$  stations for different  $N_{max}$  values (at the midpoint of the elements), the pressure coefficients of figure 10 were interpolated to a common  $x/l$  station (the trailing edge). The asymptotic approach of the pressure coefficients, lift coefficient, and center-of-pressure location to the theoretical values from reference 5 with increasing  $N_{max}$  is apparent.

— Theory of reference 4  
 ○ Numerical method

— Theory of reference 4  
 ○ Numerical method

$\beta \cot \Delta = 0.80$

$\beta \cot \Delta = 1.20$

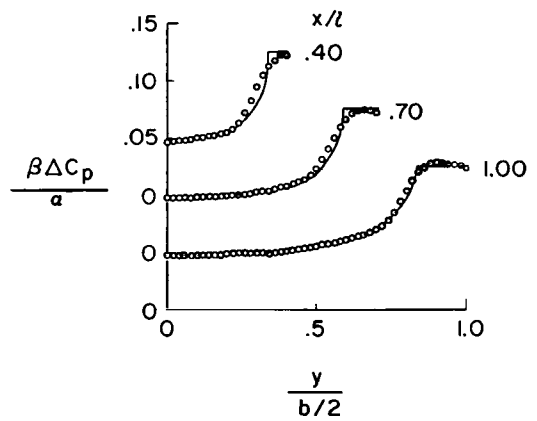
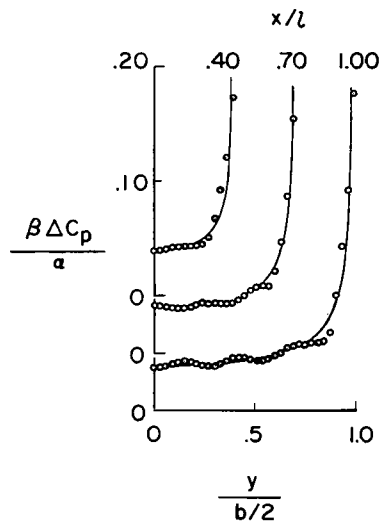
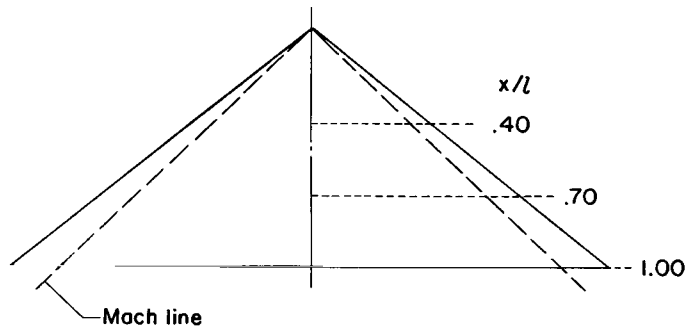
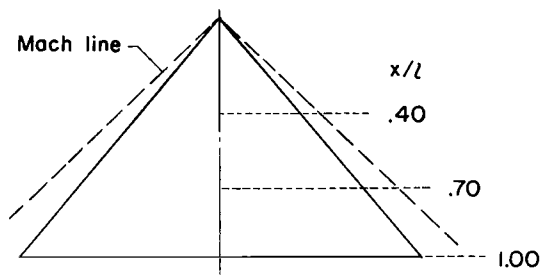


Figure 7.- Lifting-pressure distributions for subsonic leading-edge delta wing.  $N_{\max} = 50$ .

Figure 8.- Lifting-pressure distributions for supersonic leading-edge delta wing.  $N_{\max} = 50$ .

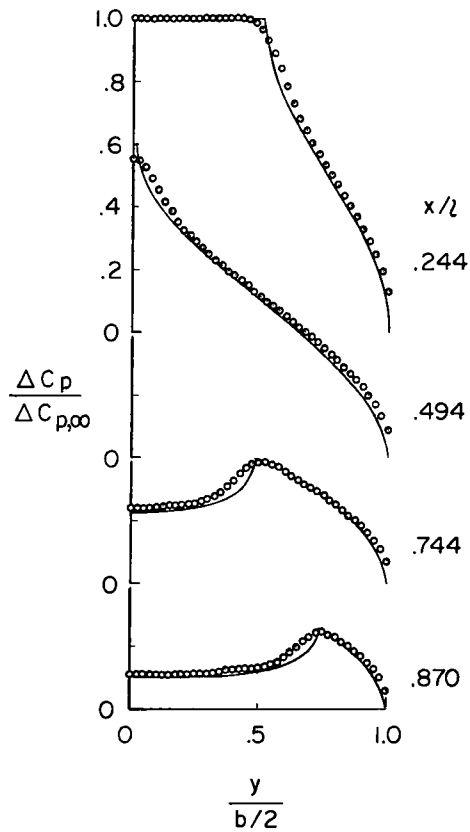
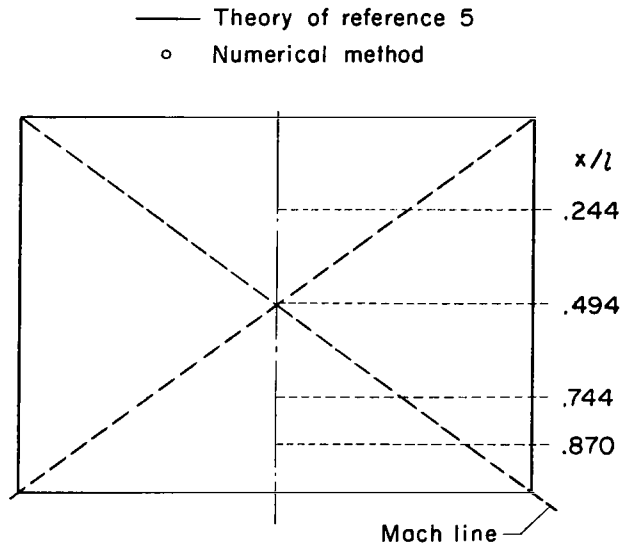


Figure 9.- Lifting-pressure distributions for rectangular wing.  $\beta AR = 1.0$ ;  
 $N_{max} = 40$ .

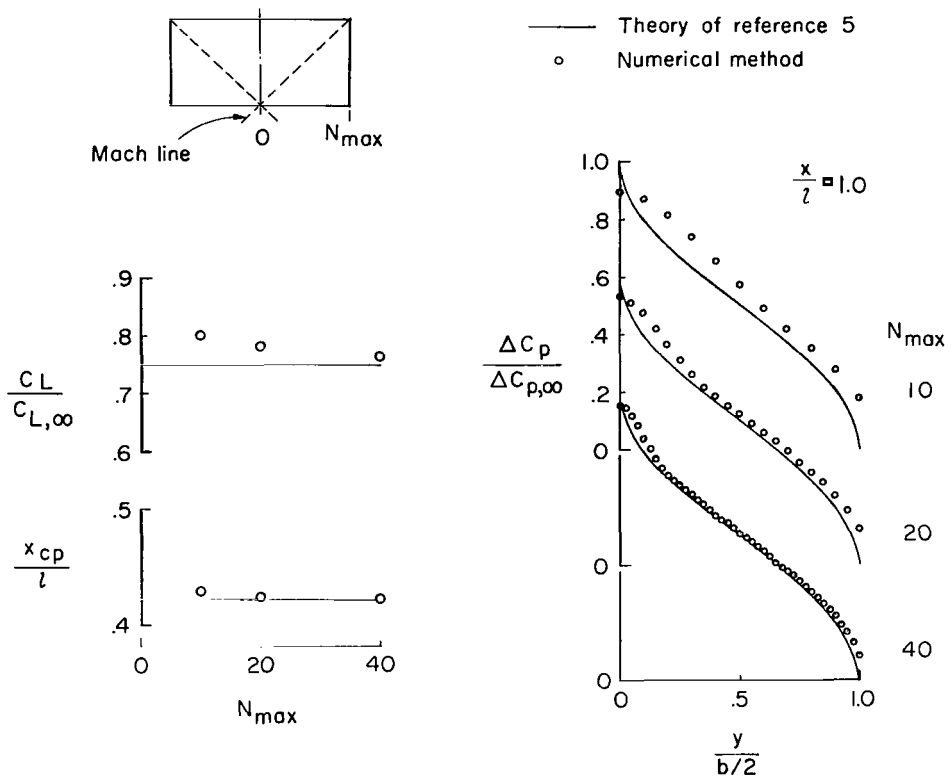


Figure 10.- Effect of  $N_{max}$  on characteristics of rectangular wing.  
 $\beta AR = 2.0$ .

Lifting-pressure distributions for a more complex planform geometry, the double-delta type, are shown in figure 11 where the numerical-method data are compared with the theoretical data obtained from the superposition solution of reference 6. For both Mach numbers ( $M = 1.414$  and  $1.667$ ), the data from the numerical method exhibit approximately the same areas under the lifting-pressure curves as the superposition solution, although no sharp peaks occur in the numerical method. A comparison of the wing force coefficients obtained by the two solutions likewise shows reasonable agreement:

	$M = 1.414$		$M = 1.667$	
	$C_{L\alpha}$	$x_{cp}/l$	$C_{L\alpha}$	$x_{cp}/l$
Superposition analysis . . . . .	0.0514	0.682	0.0461	Not given
Numerical method . . . . .	0.0507	0.687	0.0449	0.686

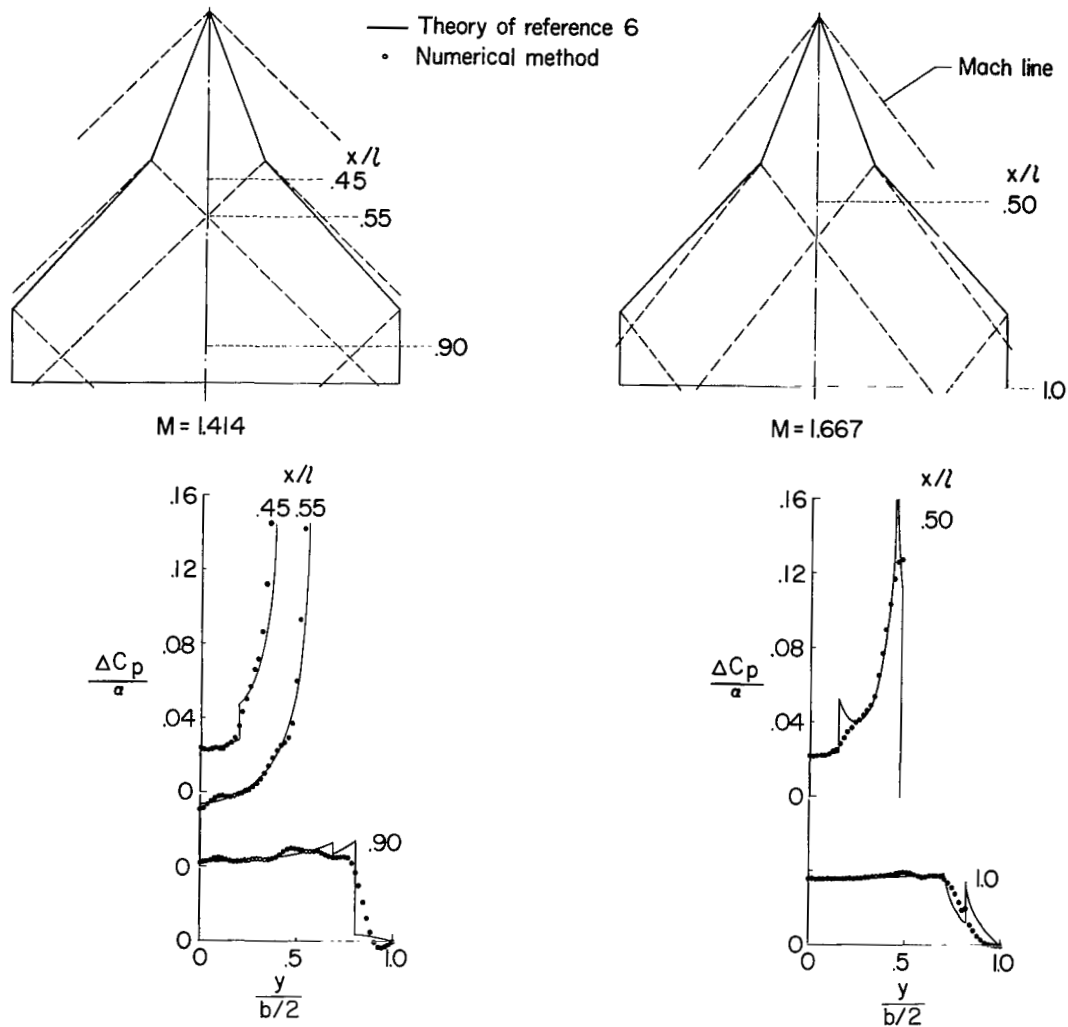


Figure 11.- Lifting-pressure distributions for double-delta wing.  $N_{max} = 50$ .

A final comparison illustrating the use of the numerical method to estimate the linear-theory characteristics of a wing family is presented in figure 12, where the lift-curve slope of a wing series having an unswept midchord and a constant taper ratio of 0.5 is shown for a Mach number of 1.53. Reasonable agreement between the numerical method and the theory of reference 7 was obtained. (In order to limit calculation time, a value of  $N_{max}$  of 25 was used for the wing with an aspect ratio of 1.)

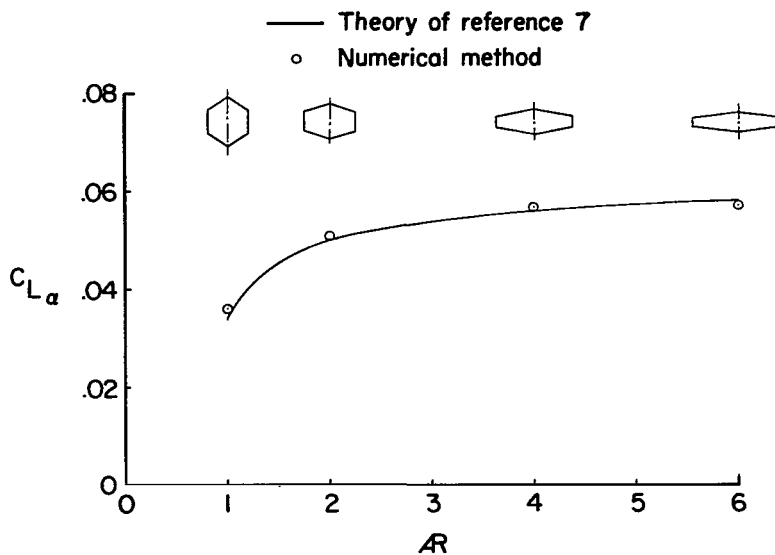


Figure 12.- Lift-curve slope of wing series having unswept midchord.  $\lambda = 0.5$ ;  $M = 1.53$ .

#### Application of Numerical Method to Wings of Arbitrary Planform

Several examples of the use of the numerical method to estimate the aerodynamic characteristics of wings having cranked or curved leading edges are presented in figures 13 to 17.

The characteristics of an M-wing planform having symmetric apexes at 0.30 semispan are illustrated in figure 13. The wing leading edge is sweptback equally on either side of the apexes, and the trailing edge is notched varying amounts. Compared with a delta wing having the same sweepback parameter (fig. 4), the M wing has a generally higher lift-curve slope for  $\beta \cot \Lambda < 1.0$ , has the same lift-curve slope for  $\beta \cot \Lambda > 1.0$  (equal to the lift-curve slope of the infinite-aspect-ratio wing), and has a center-of-pressure location forward of that of the delta wing by approximately 2 percent of the wing length. The effect of the trailing-edge notch on the M wing is to carve out a relatively low lift area, increasing the lift-curve slope of the remaining wing.

The effect of apex position on the aerodynamic characteristics of an M-wing family is shown in figure 14 for  $\beta \cot \Lambda = 0.80$ , with symmetric sweepback on either side of the apexes as before. Apex positions  $\frac{y_a}{b/2}$  of 0 and 0.53 (or greater) correspond to a single and an isolated pair of arrow wings, respectively. The effect of apex position on the lift-curve slope of the family is not large (approximately 5 percent for the unnotched planforms) and varies only slightly over a range of apex positions from 0.20 to 0.40 semispan. The corresponding shift in center of pressure is also rather small. However, an interesting effect of notching the M-wing planforms may be observed from the data of

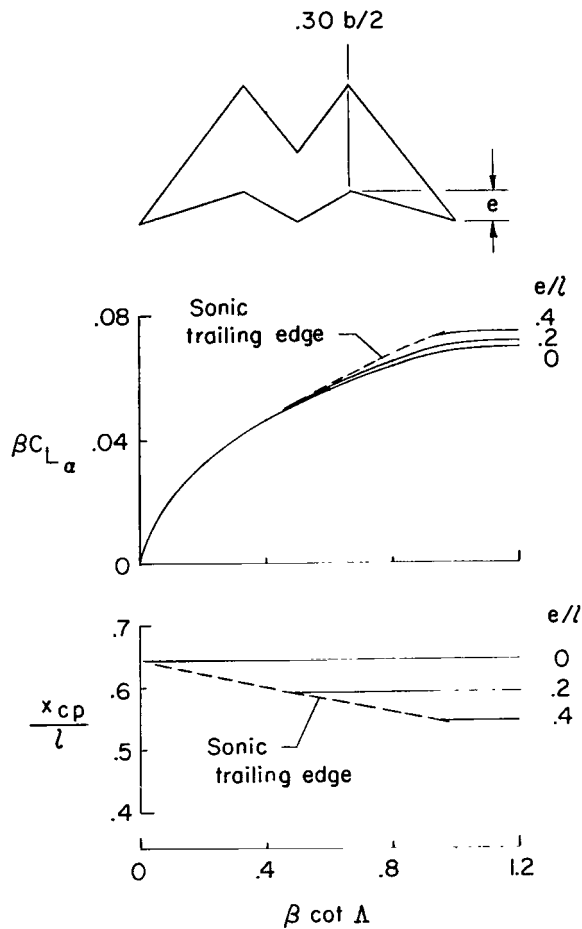


Figure 13.- Characteristics of M-wing family with apex at 0.30 semispan.

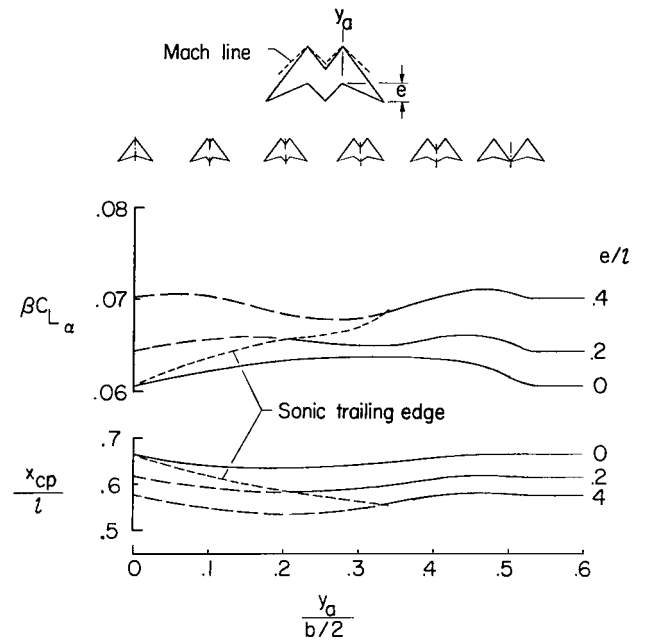
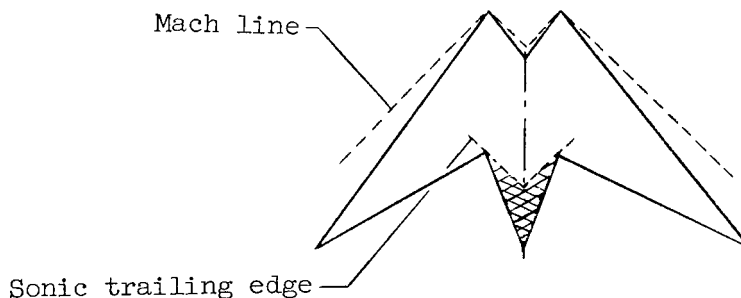


Figure 14.- Effect of apex position on characteristics of M-wing family.  $\beta \cot \Lambda = 0.80$ .

figures 14 and 15. The notch-ratio data were obtained by removing sections of the delta type of trailing edge, a process which is partially invalid because of the assumption of a supersonic trailing edge. The wing area having invalid pressure distributions is that shown cross-hatched in the sketch; the corresponding aerodynamic characteristics are indicated by dashed lines in figure 14. These data are included because of the insight offered into the pressure distributions on the M-wing planform.



The M wing with varying apex position may be alternatively regarded as a wing of fixed apex position of varying length. The cuts across the wing of figure 15 correspond to wings having apex positions of 0.53, 0.40, 0.30, 0.25, and 0.21 semispan ( $x/l = 0.22, 0.38, 0.58, 0.75,$  and  $0.96,$  respectively).

At an  $x/l$  of 0.22, the pressure distribution obtained is that of the subsonic leading-edge delta wing with large pressure coefficients along the wing leading edge. The pressure distributions for cuts at progressively higher values of  $x/l$  are characterized additionally by a pressure peak in the vicinity of the Mach line from the opposite apex. The effect of notching the M wings of intermediate length (apex at approximately 0.30 semispan) is to remove a portion of the highly loaded area near the Mach line and thereby reduce the lift-curve slope in comparison with that for notched wings having smaller (or larger) apex semispan fractions.

The aerodynamic characteristics of a wing family having an ogive type of leading edge are shown in figure 16. The leading-edge geometry is specified in the equation at the top of the figure, with  $K = 1$  giving a straight-line leading edge and  $K = 2$  defining a parabolic leading-edge shape. The wings of the family have the same span and the same chord distribution; they are sketched

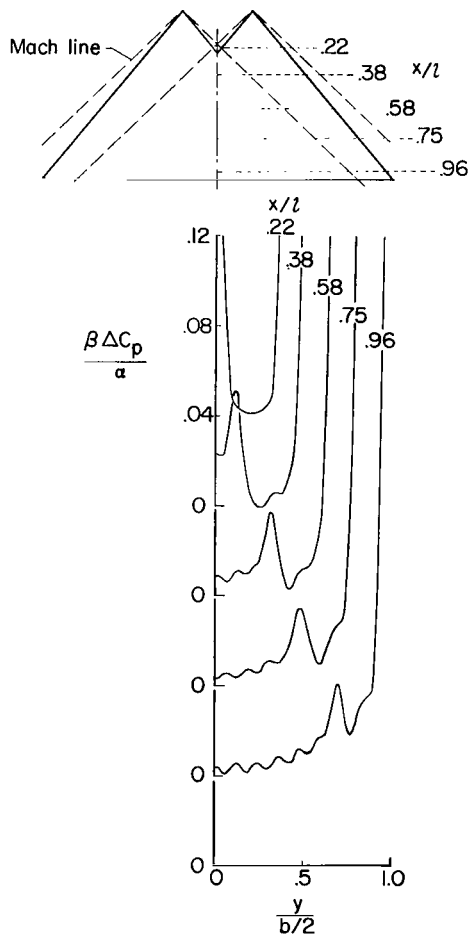


Figure 15.- Pressure distributions on M-wing planform.  $\beta \cot \Lambda = 0.80$ .

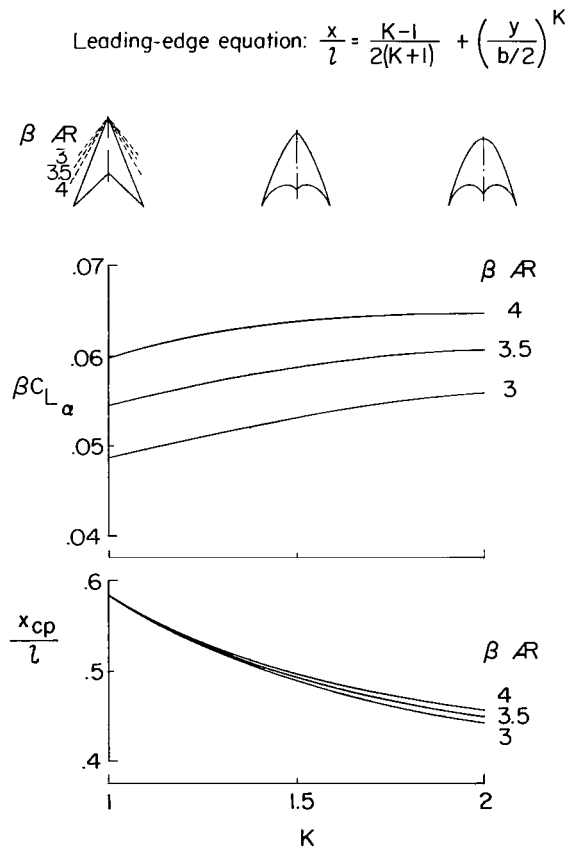


Figure 16.- Characteristics of wing family having same span and chord distribution.

for representative members having aspect ratios of 2.24. Three sweepback parameters are presented, all corresponding to a subsonic leading-edge condition for the arrow wing, as shown. The lift-curve slope of the parabolic leading-edge wing is approximately 8 percent higher than that for the arrow wing, with an accompanying large forward shift in the streamwise center of pressure.

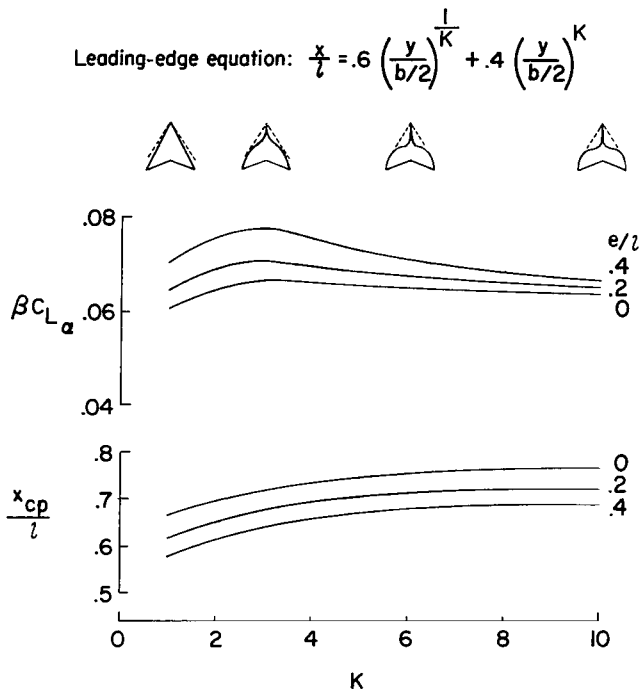


Figure 17.- Characteristics of ogee family having same span and length.  $(\beta \cot \Lambda)_{\text{Delta}} = 0.80$ .

A final example of the theoretical aerodynamic characteristics of a parametric wing family is shown in figure 17, illustrating an ogee series having the same span and length and a sweepback parameter of  $\beta \cot \Lambda = 0.80$  for the straight-line leading-edge wing. The effect of notch ratio is also shown. The center of pressure moves steadily aft with increasing  $K$ , primarily because of the aft shift in wing area. However, the wing lift-curve slope reaches a maximum at  $K \approx 3$ , and this value is approximately 10 percent higher than that for the delta or arrow wing of  $K = 1$ . As  $K$  becomes large, the wing takes on an increasingly rectangular shape with associated theoretical characteristics.

#### CONCLUDING REMARKS

A numerical method for calculating the theoretical flat-plate lifting-pressure distributions on supersonic wings of arbitrary planform, restricted only to a supersonic trailing edge, has been presented. The precision of the method was illustrated through comparisons of lifting-pressure distributions and force coefficients between the numerical method and established analytical solutions, and typical examples of the use of the method to estimate the theoretical aerodynamic characteristics of supersonic wings having curved or cranked leading edges were presented. The extension of the method to the case of cambered wings was indicated.

Langley Research Center,  
National Aeronautics and Space Administration,  
Langley Station, Hampton, Va., October 8, 1964.

## REFERENCES

1. Carlson, Harry W.; and Middleton, Wilbur D.: A Numerical Method for the Design of Camber Surfaces of Supersonic Wings With Arbitrary Planforms. NASA TN D-2341, 1964.
2. Lomax, Harvard; Heaslet, Max. A.; and Fuller, Franklyn B.: Integrals and Integral Equations in Linearized Wing Theory. NACA Rep. 1054, 1951. (Supersedes NACA TN 2252.)
3. Mangler, K. W.: Improper Integrals in Theoretical Aerodynamics. Rep. No. Aero. 2424, British R.A.E., June 1951.
4. Puckett, A. E.; and Stewart, H. J.: Aerodynamic Performance of Delta Wings at Supersonic Speeds. J. Aeron. Sci., vol. 14, no. 10, Oct. 1947, pp. 567-578.
5. Bonney, E. Arthur: Aerodynamic Characteristics of Rectangular Wings at Supersonic Speeds. J. Aeron. Sci., vol. 14, no. 2, Feb. 1947, pp. 110-116.
6. Cohen, Doris; and Friedman, Morris D.: Theoretical Investigation of the Supersonic Lift and Drag of Thin, Sweptback Wings With Increased Sweep Near the Root. NACA TN 2959, 1953.
7. Nielsen, Jack N.; Matteson, Frederick H.; and Vincenti, Walter G.: Investigation of Wing Characteristics at a Mach Number of 1.53. III - Unswept Wings of Differing Aspect Ratio and Taper Ratio. NACA RM A8E06, 1948.

2/1/58

*"The aeronautical and space activities of the United States shall be conducted so as to contribute . . . to the expansion of human knowledge of phenomena in the atmosphere and space. The Administration shall provide for the widest practicable and appropriate dissemination of information concerning its activities and the results thereof."*

—NATIONAL AERONAUTICS AND SPACE ACT OF 1958

## NASA SCIENTIFIC AND TECHNICAL PUBLICATIONS

**TECHNICAL REPORTS:** Scientific and technical information considered important, complete, and a lasting contribution to existing knowledge.

**TECHNICAL NOTES:** Information less broad in scope but nevertheless of importance as a contribution to existing knowledge.

**TECHNICAL MEMORANDUMS:** Information receiving limited distribution because of preliminary data, security classification, or other reasons.

**CONTRACTOR REPORTS:** Technical information generated in connection with a NASA contract or grant and released under NASA auspices.

**TECHNICAL TRANSLATIONS:** Information published in a foreign language considered to merit NASA distribution in English.

**TECHNICAL REPRINTS:** Information derived from NASA activities and initially published in the form of journal articles.

**SPECIAL PUBLICATIONS:** Information derived from or of value to NASA activities but not necessarily reporting the results of individual NASA-programmed scientific efforts. Publications include conference proceedings, monographs, data compilations, handbooks, sourcebooks, and special bibliographies.

*Details on the availability of these publications may be obtained from:*

SCIENTIFIC AND TECHNICAL INFORMATION DIVISION  
NATIONAL AERONAUTICS AND SPACE ADMINISTRATION  
Washington, D.C. 20546